RSC Advances

Role of counter-ion and helper lipid content in the performance of nanocarrier systems: a biophysical study in 2D and 3D lipid assemblies

Journal:	*RSC Advances*
Manuscript ID	Draft
Article Type:	Paper
Date Submitted by the Author:	n/a
Complete List of Authors:	Oliveira, Ana; CFUM, Centre of Physics of University of Minho, Department of Physics; CBMA, Centre of Molecular and Environmental Biology of University of Minho, Department of Biology Nogueira, Sara; CFUM, Centre of Physics of University of Minho, Department of Physics Gonçalves, Odete; CFUM, Centre of Physics of University of Minho, Department of Physics; CBMA, Centre of Molecular and Environmental Biology of University of Minho, Department of Biology Fátima Cerqueira, M.; CFUM, Centre of Physics of University of Minho, Department of Physics Alpuim, Pedro; CFUM, Centre of Physics of University of Minho, Department of Physics; INL, International Iberian Nanotechnology Laboratory, Nanoelectronics Tovar, Júlia; CFUM, Centre of Physics of University of Minho, Department of Physics Rodriguez-Abreu, Carlos ; INL, International Iberian Nanotechnology Laboratory, Nanomachines & Nanomanipulation Brezesinski, Gerald; MPI-KG, Max Planck Institute of Colloids and Interfaces, Colloids and Interfaces Gomes, Andreia; CBMA, Centre of Molecular and Environmental Biology of University of Minho, Department of Biology Lúcio, Marlene; CFUM, Centre of Physics of University of Minho, Department of Physics Cunha Dias Real Oliveira , Maria Elisabete; CFUM, Centre of Physics of University of Minho, Department of Physics
Subject area & keyword:	Biophysics - Physical < Physical

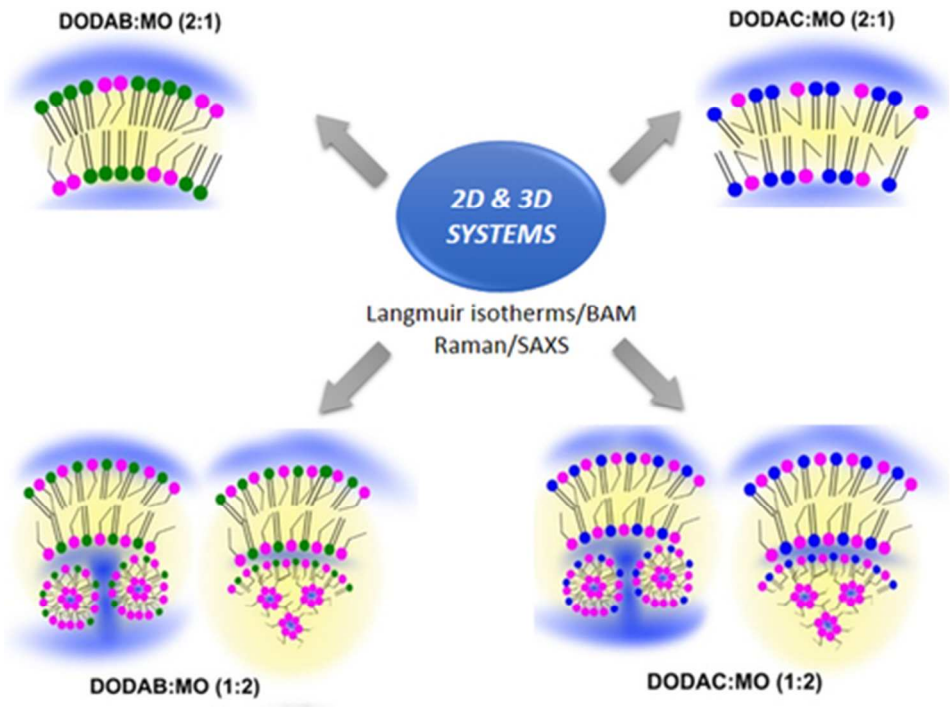

39x29mm (300 x 300 DPI)

RSC Advances

ARTICLE

Role of counter-ion and helper lipid content in the performance of nanocarrier systems: a biophysical study in 2D and 3D lipid assemblies

Received 00th January 20xx,
Accepted 00th January 20xx

DOI: 10.1039/x0xx00000x

www.rsc.org/

Ana C. N. Oliveira[a,b], Sara S. Nogueira[b,c], Odete Gonçalves[a,b], M. F. Cerqueira[b], P. Alpuim[b,d], Júlia Tovar[b], Carlos Rodriguez-Abreu[d], Gerald Brezesinski[c], Andreia C. Gomes[a], Marlene Lúcio[b*], M.E.C.D. Real Oliveira[b]

There is a direct correlation between physicochemical properties of nanocarrier systems and their biological performance, including stability in physiological conditions, cellular internalization and transfection efficiency. Therefore, understanding the biophysical aspects that affect self-assembled nanocarriers is determinant for a rational design of efficient formulations. In this study, a comprehensive evaluation of the effects of each component on the molecular organization of aggregates formed by the cationic lipids dioctadecyldimethylammonium bromide and chloride (DODAB and DODAC) and the neutral lipid monoolein (MO) was made. Specifically, the effects of the *helper* lipid content (MO) and the role of the counter-ion of the cationic lipids were evaluated in 2D and 3D assemblies by Langmuir surface pressure-molecular area (π-A) isotherms, Brewster Angle Microscopy (BAM), Infrared Reflection Absorption Spectroscopy (IRRAS), Confocal Raman Microscopy, and Small Angle X-ray Scattering (SAXS). Results show that MO has a different distribution on DODAC and DODAB bilayers, and a fluidizing effect dependent on the MO content. For low MO molar ratios, the fluidizing effect was more pronounced in DODAC:MO mixtures, indicating a more homogeneous distribution of MO in DODAC than in DODAB bilayers. For high MO molar ratios, packing of membranes was similar for both cationic lipids, and the effect of the counter-ion is attenuated. The distribution of MO in the two cationic systems is closely related with the efficiency of the counter-ions in the screening of the charged group.

Introduction

Liposomes have been extensively explored as drug and genetic material delivery systems.[1, 2] Cationic liposomes, for instance, are largely used for gene delivery purposes because they promote compaction of nucleic acids by electrostatic interactions between the positive charges of cationic lipids and the negative charges of phosphate backbones.[3] Neutral (*helper*) lipids are usually included in cationic liposomal formulations to: help nucleic acids escaping from the endosomes[4-6]; aid nucleic acids complexation[7]; decrease toxicity associated with cationic lipids[2]; or confer more favourable properties in terms of fluidity of the lipid aggregates.[8, 9] Cholesterol and 1,2-dioleoyl-*sn*-glycero-3-phosphoethanolamine (DOPE) are the most commonly used helper lipids, but monoolein (MO) also shows promising results in formulations developed for gene therapy.[10-18] MO is a neutral lipid that has a low solubility in water but easily swells in contact with an aqueous phase. MO exhibits a lyotropic behaviour forming various lipid phases depending on the temperature and water content, including lamellar (L_α), inverted hexagonal (H_{II}), and bicontinuous cubic (Q_{II}^D and Q_{II}^G) phases.[19, 20] The rich polymorphism of MO, in particular its capacity to form inverted bicontinuous cubic phases in excess water, consisting of two intertwined but not interpenetrating water channels separated by a lipid bilayer surface, offers the possibility to entrap hydrophilic substances in the water channels, lipophilic compounds in the lipid bilayer, and amphiphilic substances.[20-22] Besides increasing the entrapment capacity of chemically different payloads, MO inverted non-lamellar phases allow controlling the release of those payloads by a slow diffusion process.[20, 22, 23] Hence, MO can be a very interesting *helper* lipid in nanostructured lipid carriers for nucleic acid and/or drug delivery purposes.

Liposomes composed of MO and lipids from the dioctadecyldimethylammonium family (DODAX, where X stands for Br or Cl) have shown to be efficient nucleic acid delivery systems.[12-18, 24] Dioctadecyldimethylammonium bromide (DODAB) and

[a] CBMA (Centre of Molecular and Environmental Biology), Department of Biology, University of Minho, Campus of Gualtar, 4710-057 Braga, Portugal.
[b] CFUM (Centre of Physics), Department of Physics, University of Minho, Campus of Gualtar, 4710-057 Braga, Portugal.*mlucio@fisica.uminho.pt
[c] Max Planck Institute of Colloids and Interfaces, Science Park Potsdam-Golm, 14476 Potsdam, Germany
[d] INL (International Iberian Nanotechnology Laboratory), Av. Mestre José Veiga, 4715-330 Braga, Portugal

† Footnotes relating to the title and/or authors should appear here.
Electronic Supplementary Information (ESI) available: [details of any supplementary information available should be included here]. See DOI: 10.1039/x0xx00000x

chloride (DODAC) assemble into bilayer structures when dispersed in aqueous media above the phase transition temperature.[25] Although only differing in the counter-ion, they form vesicles that after conjugation with nucleic acids originate lipoplexes with different characteristics. Indeed, DODAB:MO and DODAC:MO lipoplexes were tested for gene delivery purposes and compared in terms of gene knockdown, toxicity, and stability in human serum.[26] Important differences were found between the biological activities of both systems[26], but the explanation for these differences remains elusive, although it seems evident that differences in physical organization of lipid transfection agents may affect their biological outcome.

The main goal of this study is to compare the effects of MO on DODAB and DODAC structural organization, by evaluating the influence of the cationic lipid:neutral lipid molar ratio as well as the effect of the counter-ions on the overall aggregate structure. To our knowledge, this is the first report on the effects of *helper* lipid content and counter-ion effect on DODAX lipid transfection agents. The structural aspects of DODAX:MO prepared in systems of different dimensionality (two-dimensional (2D) and three-dimensional (3D) membrane models) will also be compared since the molecular organization in different dimensions can provide complementary information on distinct parameters. In 3D spherical membrane mimetic systems (e.g. liposomes), membrane parameters such as packing density, mobility of the molecular components, and topology of the surfaces are simultaneously affected by interactions between the lipid components, and it is very difficult to extract individual contributions of any of these parameters. In this context, 2D membrane models, such as Langmuir monolayers at the soft air/liquid interface, complement the information gathered with 3D lipid models. At the same time, 2D systems provide many possibilities to control, in an effective way, a wide range of experimental variables, such as the phase state of the film-forming molecules, packing density and compressibility of the molecules. Nevertheless, although Langmuir monolayers are excellent model systems for the study of order and packing of lipids in two dimensions[27] some properties like miscibility, phase equilibrium, hydration or dynamics might be different for 2D monolayer and 3D multilayer systems.[28] This reinforces the importance of using different techniques to confirm and complement results obtained in lipid organizations of different dimensionality. Therefore, we have evaluated DODAX:MO monolayers in 2D assemblies by Langmuir isotherms, Brewster Angle Microscopy (BAM) and Infrared Reflection Absorption Spectroscopy (IRRAS in supplementary information) and the results were compared with those obtained in 3D assemblies studied by Confocal Raman microscopy and Small Angle X-ray Scattering (SAXS).

Experimental

Materials

Dioctadecyldimethylammonium bromide (DODAB) (purity > 98.0 %), dioctadecyldimethylammonium chloride (DODAC) (purity > 97.0 %) and 1-monooleoyl-*rac*-glycerol (MO) (purity > 99.0 %) were purchased from Sigma-Aldrich (Bornem, Belgium), and used without further purification. Fig. 1 shows the chemical structure of the lipids.

PLEASE INSERT FIGURE 1

Methods

Surface pressure-molecular area (π-A) isotherms and Brewster Angle Microscopy (BAM)

Monolayers of DODAX and DODAX:MO at molar ratios (1:2) and (2:1) were studied as 2D membrane model systems. Surface pressure-molecular area isotherms (π-A) were measured in a PTFE Langmuir trough (Riegler & Kirstein, Potsdam, Germany), equipped with barriers for changing the surface area, and a Wilhelmy microbalance with filter paper plate (accuracy superior to 0.1 mN/m) for measuring the surface pressure of the monolayer.

Monolayers were obtained after spreading lipid solutions (1 mM in chloroform) on the aqueous subphase. After an equilibration time of 10 min, the monolayers were compressed at a rate of 5 $Å^2$/molecule/min. Before each measurement, the trough was cleaned thoroughly with chloroform and double-deionized water. Cleanliness was confirmed by compressing a water subphase and achieving a zero surface pressure reading. All measurements were performed at 20 °C.

To study the morphology of lipid monolayers, a Brewster Angle Microscope (BAM2plus from NanoFilm Technologie, Göttingen, Germany) was combined with a Langmuir Film Microbalance (NIMA Technology Ltd, United Kingdom) placed on an anti-vibration table. The beam coming from frequency-doubled Nd:YAG laser (532 mm, 50 mW) passed through a polarizer and hits the surface under an incidence angle of 53.1°. The reflection was captured by an analyzer combined with a CCD camera (image size 355x470 μm^2, resolution approximately 2 μm).

Confocal Raman Microscopy

Confocal Raman microscopy was used to study the interaction of DODAX and MO lipids in a 3D assembly. Liposomes were prepared either with DODAB or DODAC and the neutral lipid MO by the lipid film hydration method. Briefly, defined volumes of DODAX and MO (20 mM in ethanol) were added to a round-bottomed flask and the solvent evaporated under vacuum (30 min at 40 °C). Subsequently, ultrapure water (temperature > 50 °C) was added to the lipid film, and liposomes DODAX:MO (2:1) or DODAX:MO (1:2) (mol:mol) were formed at 3 mM.

Raman scattering experiments of DODAX:MO (2:1) and DODAX:MO (1:2) were performed at room temperature (20 °C) in a back scattering geometry on alpha300 R confocal Raman microscope (WITec), using a 532 nm Nd:YAG laser for excitation. The laser beam was focused on the sample by a x50 lens (Zeiss); the spectra were collected with a 600 groove/mm grating using 10 acquisitions with a 2 s acquisition time. Lorentzians were fitted to the vibrational bands in the Raman spectra, and the peak positions and corresponding full-width at half-maximum (FWHM) were determined.

Small Angle X-ray Scattering (SAXS)

Liposomes were prepared at 40 mM by the already described thin film hydration method. After hydration with ultrapure water, liposomes were subjected to 3 alternating cycles of heating (10 min, 60 °C) and vortexing (5 min), after which they were centrifuged (30 s at 2000 g). Samples were aged overnight at 4 °C, and before dispersions were transferred into glass capillaries, a vortexing cycle of 5 min was performed. Glass capillaries with 0.9 mm in diameter and 0.01 mm wall thickness (Hilgenberg, Malsfeld, Germany) were used. The flame-sealed capillaries were stored at 4 °C until measurements were made. SAXS experiments were performed in an Anton Paar SAXSess mc2 instrument with an image plate detector. Samples were allowed to equilibrate for 5 min before the diffraction pattern was recorded at 20 °C. Lorentzians were fitted to the diffraction peaks, and the positions of maximum intensities and the full-widths at half-maximum (FWHM) of the peaks were determined. FWHM values were used to calculate the correlation length between the lipid bilayers ($\xi = 2\pi/FWHM$). Bragg distances were calculated as $d=2\pi/q$, where q is the scattering vector at the corresponding SAXS peak.

Results and discussion

Understanding the key parameters influencing processes such as formation and disassembly of lipoplexes, as well as colloidal stability in physiological conditions are determinant to the rational design of highly efficient nanosystems for gene therapy.

Lipoplexes composed by DODAX:MO have been previously reported to induce dissimilar biological responses (e.g. gene silencing efficiency) and to have different colloidal stability in human serum.[26] Moreover, DODAX:MO liposomes have shown different siRNA complexation profiles (Fig. S1 – supplementary information).

The different biological responses observed motivated the need to perform a detailed study of the influence of the counter-ion and MO content on the biophysical properties of DODAX:MO based formulations. In this regard, the current biophysical study is based on a multi-technique approach to clarify the differences observed between the various DODAX:MO aggregates, by the analysis of lipid structures with different dimensionality (2D by Langmuir isotherms, BAM, IRRAS and 3D by Confocal Raman microscopy and SAXS).

Analysis of DODAX:MO mixtures in 2D assemblies by Langmuir isotherms and BAM

The structures of neat DODAB and DODAC monolayers at the air–water interface have been reported before,[29-33] however, to our knowledge, there is no comparative study on the influence of the helper lipid MO on these cationic lipids. Although the effect of MO on the conformation of DODAB molecules has been already investigated,[24] that study was not sufficient to clearly explain the different transfection and serum stability behaviours observed for DODAX:MO lipoplexes[26] (Fig. S1 – supplementary information). Therefore, our previous study[24] was extended also to DODAC and to different MO ratios. Accordingly, the surface pressure–molecular area (π-A) isotherms of DODAX:MO monolayers at the air–water interface were obtained for several DODAX:MO compositions, at (20.0 ± 0.2) °C, in order to monitor differences in the interfacial molecular organization of the lipids (Fig. 2A).

PLEASE INSERT FIGURE 2

The π–A isotherm obtained for DODAB is in agreement with previously reported isotherms prepared under the same conditions, i.e. aqueous subphase and 20 °C [30, 31] and exhibits three distinct regions: a liquid-expanded (LE) phase, at low surface pressures and large areas per molecule; a liquid-expanded/liquid-condensed (LE–LC) phase transition region; and a liquid-condensed (LC) phase at areas per molecule of less than 60 $Å^2$ and high surface pressures, before the collapse near 47 mN/m (Fig. 2A – dashed purple line).

The π–A isotherm obtained for DODAC presents a LE phase similar to DODAB, but the transition region cannot be seen (Fig. 2A – pink line), and the areas per molecule at higher pressures are clearly larger compared to DODAB. Hence, in comparison to the LC phase of DODAB, DODAC forms rather a liquid-ordered phase. These results are supported by the IRRAS experiments (Fig. S2 - supplementary Information). The phase transition from LE to LC in DODAB monolayers is connected with a jump in the wavenumbers of the CH_2- stretching vibrations to lower values. E.g., the asymmetric stretching vibration band is observed at 2925 cm^{-1} in the LE phase and 2920 cm^{-1} in the LC phase (Fig. S2 - supplementary Information). The situation is different with DODAC. As in the isotherms, the transition to the LC phase cannot be observed as a jump in wavenumbers (fist-order transition), instead of that, the wavenumbers decrease continuously with increasing pressure. At the highest lateral pressure measured, the wavenumbers of DODAC are at least 1 cm^{-1} larger than those of DODAB indicating a less dense packing (Fig. S2 - supplementary Information). Therefore, the change of the counter-ion (from bromide to chloride ions) has a big influence on the type of the transition (second-order instead of first-order) and on the packing density in the monolayer at high-pressure. Chloride ions have a larger hydration shell than bromide ions, and consequently they are not as tightly connected to the charged lipid head group and screen less effectively the cationic charge in the head group region.[34-36] This assumption is strongly supported by our previous work using a long-chain sulfate on subphases containing different cations.[37] In this work we have shown that the size of counter-ions affects the electrical double layer (EDL). Therefore, the electrostatic term of the free energy of the total system (monolayer + subphase) appears to be dependent on the counter-ion size for highly charged monolayers. In the presence of two different counter-ions, preferential participation of the smaller one in the EDL formation is favourable in terms of free energy. In the present case, since chloride ions are effectively larger, the DODAC monolayers are dominated by stronger electrostatic repulsions between the charged head groups leading to a less dense packing (supported by the higher CH_2 wavenumbers at high pressures observed in Fig. S2 - supplementary Information) compared to DODAB. To illustrate this effect more clearly, DODAB

and DODAC have been measured on 10 mM NaBr or NaCl solutions, respectively. In the case of DODAB, the phase transition region (coexistence of LE and LC) is seen as a perfect horizontal plateau at ≈2 mN/m, whereas DODAC on the 10 mM NaCl solution does not exhibit any plateau but the area decreases continuously with increasing pressure (Fig. S3 - supplementary Information). In the LC phase, the DODAB chains are strongly tilted (≈ 34° to the surface normal on a 2 mM NaBr containing subphase) due to the electrostatic repulsions of the positively charged head groups.[38] Above 20 mN/m, the molecular area of DODAC is even smaller than that of DODAB. Therefore, it is assumed a liquid-ordered phase with almost perpendicular orientation of the DODAC chains, which must have a larger cross-sectional area than the ones of DODAB (as confirmed by the higher wavenumbers of the CH_2 stretching vibration seen in Fig. S2 - supplementary Information) indicating a less dense packing.

MO monolayer (Fig. 2A – blue line) agrees well with previously reported data[39] and has the typical shape of a LE phase of single-chain amphiphiles, but the molecular areas are smaller than expected. MO is highly hygroscopic. Therefore, the molecular areas determined in the isotherms are apparent because of an effectively lower concentration of MO molecules in the spreading solution.

The addition of small amounts of MO to the DODAB monolayer (molar ratio 2:1) caused a shift in the isotherm towards a smaller average molecular area and the disappearance of the phase transition region. However a change of slope close to 30 mN/m indicates the transition into the LC phase (Fig. 2A purple dashed-dotted line).

The isotherm of the DODAC:MO (2:1) monolayer is located at larger areas per molecule (Fig. 2A pink dashed-dotted line) compared to the isotherm of DODAB:MO (2:1). The increase in the area per molecule of DODAC:MO (2:1) when compared to DODAB:MO (2:1) can be explained by the progressive screening of the monolayer surface charge and is consistent with the assumption that DODAC molecules are effectively more positively charged (due to the reduced screening capacity of the larger chloride ion in the hydrated state, which is less tightly bound to the charged head group in the inner Helmholtz plane) than DODAB molecules. Thus, DODAC has a less ordered polar region due to stronger repulsive forces between the positively charged lipid head groups. Oppositely, DODAB forms bilayers more densely packed at the head group region than DODAC. These different packing characteristics influence how MO is incorporated as a *helper* lipid into the monolayers of these cationic lipids. Plotting the molecular areas versus the mole fraction of MO indicates a non-ideal mixing between DODAB and MO at 2:1 molar ratio. On the other hand, MO eased insertion within DODAC monolayers is confirmed as the molecular areas of these two lipids as a function of the mole fraction points to an ideal mixing (data not shown).

The isotherms of the monolayers DODAC:MO (1:2) and DODAB:MO (1:2) are almost superimposed (Fig. 2A pink dotted line and purple dotted line), thus changing the counter-ion from chloride to bromide does not seem to have a significant influence on the monolayer structure at high MO contents.

The phase behaviour of the monolayer is better seen when looking at the dependence of the compression modulus (Cs^{-1}) on the area per molecule (Fig. 2B). According to the literature[40], the variation of the Cs^{-1} reflects the monolayer phase transitions and three distinct regions can be observed. The regions with low Cs^{-1} at large area per molecule correspond to LE phases, whereas the regions with high Cs^{-1} at small areas per molecule correspond to LC phases. These regions are separated by a pronounced drop of the compression modulus correspondent to the LE-LC coexistence region. Accordingly, DODAB forms the least compressible monolayer (highest C_S^{-1} max), confirming that this monolayer also presents the highest head group ordering. The most compressible monolayer is DODAC:MO (2:1) (smallest C_S^{-1} max). DODAB-monolayers show higher C_S^{-1} max than DODAC-monolayers for the same cationic lipid:neutral lipid molar ratio. However, when MO is in excess (molar ratio 1:2), the value is the same for both systems. Monolayers containing higher contents of MO (DODAX:MO molar ratio 1:2) are not very different in terms of compressibility when compared to the neat MO monolayer.

Since DODAB was the only monolayer forming the LE, LE+LC and LC phases, BAM images are shown for this composition in Fig. 2C. At maximum expansion, a 2D foam often appears for the DODAB monolayer, and a homogeneous BAM image is recovered after the lift-off point at a low surface pressures (Fig. 2C, LE). BAM images of the DODAB monolayer revealed the presence of small domains showing 'bubble-like' features (Fig. 2C, LE+LC), that progressively became more densely packed (Fig. 2C, LC) until the image gets homogeneous upon further compression (data not shown). This behaviour indicates a large nucleation rate and a slow growth of the condensed domains which makes difficult to compare the shape of the domains in the different mixed monolayers. However it is possible to observe that at the smaller MO contents (DODAX:MO (2:1)) the same type of domains appeared for DODAB:MO while the mixed DODAC:MO monolayer appeared homogeneous when visualized by BAM (Fig. S4 - supplementary Information). This confirms that MO is more homogeneously distributed in the case of DODAC, but forms phase-separated DODAB- and MO-enriched domains in DODAB aggregates.

Analysis of DODAX:MO mixtures in 3D assemblies by Confocal Raman Microscopy

Raman spectra of DODAC:MO (2:1), DODAB:MO (2:1), DODAC:MO (1:2) and DODAB:MO (1:2) liposome dispersions are shown in Fig. 3 for the range between 1000-3100 cm^{-1}.

PLEASE INSERT FIGURE 3

The Raman spectra obtained are in good agreement with the reported for other lipid composition showing the ν(C-H), ν(C-C) and δ(C-H) vibration modes.[41]

The most relevant vibrational mode frequencies, obtained after fitting each Raman spectrum, are shown in Table 1. For better clarity, 3 regions of the spectra (R1, R2 and R3) were defined and analysed separately: R1 (1050 – 1150 cm^{-1}) comprising the ν(C-C)

stretching vibrations, R2 (1200 – 1500 cm^{-1}) comprising the $\delta(CH_2)$ deformation vibrations, and R3 (2800 – 3100 cm^{-1}) corresponding to the ν(C-H) stretching vibrations, which dominate the spectra.

PLEASE INSERT TABLE 1

Fig. 3 shows that all the vibration modes were more intense for DODAX:MO liposomes prepared at the (2:1) molar ratio (Fig. 3A, 3B) when compared to the (1:2) molar ratio (Fig. 3C, 3D).

The ν(C-C) stretching mode (in region R1) reflects intramolecular *trans*/*gauche* conformational changes within hydrocarbon chains. According to the literature[41-44] the out-of-phase aliphatic C-C stretch *all-trans* vibrations $\nu(C\text{-}C)_T$ are observed between 1060-1065 cm^{-1}; the C-C stretch *gauche* vibrations $\nu(C\text{-}C)_G$ correspond to the Raman mode at ≈1086 cm^{-1}; and the in-phase aliphatic C-C stretch *all-trans* vibrations $\nu(C\text{-}C)_{ip}$ appear between 1100-1135 cm^{-1}.

Fig. 3 shows that the lipid systems with 2:1 molar ratios DODAB:MO (B spectra) and DODAC:MO (A spectra) present a well-defined Raman band assigned for $\nu(C\text{-}C)_T$ at 1066 cm^{-1}, however being shifted to higher wavenumbers and broadened for DODAC:MO (2:1) liposomes. This $\nu(C\text{-}C)_T$ band presents very low intensity in both lipid mixtures containing higher MO content (molar ratio 1:2). The $\nu(C\text{-}C)_G$ vibration peak appeared poorly defined for DODAB:MO (2:1) (1084 cm^{-1}) and DODAC:MO (2:1) (1083 cm^{-1}), and again presented very low intensity for lipid mixtures containing higher MO content.

The $\nu(C\text{-}C)_{ip}$ modes in the range 1100 and 1135 cm^{-1}, corresponding to the in-phase aliphatic C-C stretch *all-trans*, were well-defined for the lipid systems with 2:1 molar ratios DODAB:MO (B spectra) and DODAC:MO (A spectra), however, the low frequency mode is shifted (to lower wavenumbers) and broadened for DODAC:MO (2:1). The contribution of $\nu(C\text{-}C)_{ip}$ vibrations was almost irrelevant for DODAX:MO (1:2) liposomes.

The Raman spectrum in the R2 region (1200 to 1500 cm^{-1}) corresponds to the C-H deformation vibrations $\delta(CH_2)$. These modes are very sensitive to lipid chain architecture and lateral packing. The methylene twisting deformation vibrations $\delta(CH_2)_{tw}$ are observed between 1295-1305 cm^{-1}, and the methylene scissor deformation vibrations $\delta(CH_2)_{sc}$ between 1400-1500 cm^{-1}. [42]

As seen in Fig. 3, the $\delta(CH_2)_{tw}$ mode is well defined for DODAB:MO (2:1) and DODAC:MO (2:1), but the peak position was shifted and the mode is broader for the latter (peaks at 1301 cm^{-1} and 1305 cm^{-1}, respectively). Moreover, this peak is very weak for lipid mixtures containing higher MO content (molar ratio 1:2) indicating that the lateral packing is very much reduced at high MO contents.

The $\delta(CH_2)_{sc}$ (1400-1500 cm^{-1}) modes were also well-defined for DODAX:MO (2:1). It is interesting to note the intensity inversion between the 1301 cm^{-1} ($\delta(CH_2)_{tw}$) and 1400-1500 cm^{-1} ($\delta(CH_2)_{sc}$) modes, when comparing DODAB:MO (2:1) and DODAC:MO (2:1), as well as the red and blue shift of the peak position for DODAC:MO (2:1).

The C-H stretching vibration region R3 (2800-3100 cm^{-1}) is the most sensitive region and the $\nu(CH_2)$ vibrations are usually used to monitor the changes in the lipid chain lateral packing, or order/disorder properties.[45] The Raman spectra intensity in the region R3 was higher for DODAC:MO (2:1), followed by DODAB:MO (2:1), while it was very low and poorly defined for the mixtures with higher MO content (molar ratio 1:2), as observed in the others vibrational ranges. The methylene symmetric stretching vibration ($\nu_s(CH_2)$) appeared at 2855 cm^{-1} and maintained its position for all the samples, although the intensity decreased in the order DODAC:MO (2:1) > DODAB:MO (2:1) > DODAX:MO (1:2). The $\nu_s(CH_3)$ vibration mode at 2935 cm^{-1} was better defined for DODAC:MO (2:1) while the $\nu_a(CH_3)$ vibration mode at ≈ 2963 cm^{-1} was better defined for DODAB:MO (2:1). These two contributions seemed irrelevant for formulations with higher MO content.

Ratios between defined peaks of Raman spectra provide information regarding different bilayer characteristics. For example, the peak intensity ratio $[Iv C\text{-}C_G/Iv C\text{-}C_T]$ indicates the relative number of *gauche* and *trans* conformers, and thus it can be used to monitor changes in membrane order for the C-C stretching mode region.[41] The $[Iv_aCH_2/Iv_sCH_2]$ peak height intensity ratio is a measure of lateral packing density of alkyl chains and an indicator of conformational order, reflecting deviations from a perfect *all-trans* conformation.[45, 46] The ratio lies between 0.6 – 0.9 for alkanes in the liquid state, and between 1.6 and 2.0 for the crystalline state.[47, 48] Also, the higher the ratio, the more ordered the hydrocarbon chains.[49] The $[Iv_sCH_3/Iv_sCH_2]$ peak height intensity ratio is correlated to the chain coupling (intermolecular interactions) of alkyl chains.[50] This ratio is sensitive to intermolecular chain interactions and also reflects the mobility of the terminal methyl group of the hydrocarbon chains.

Fig. 4 shows the intensity ratio $[Iv C\text{-}C_G/Iv C\text{-}C_T]$ as a function of $[Iv_aCH_2/Iv_sCH_2]$, and $[Iv_sCH_3/Iv_sCH_2]$ as a function of $[Iv_aCH_2/Iv_sCH_2]$.

PLEASE INSERT FIGURE 4

Fig. 4A indicates how the number of *gauche* conformers is related to the lateral packing density of the acyl chains. A higher $[Iv C\text{-}C_G/I\ vC\text{-}C_T]$ ratio reflects a decrease in the order of the acyl chains, since it indicates an increase in *gauche* conformers. Contrarily, a higher $[Iv_aCH_2/Iv_sCH_2]$ ratio indicates an increase in conformational order. DODAB:MO (2:1) presented the lowest value of $[Iv C\text{-}C_G/Iv C\text{-}C_T]$ (0.75) and the highest value of $[Iv_aCH_2/Iv_sCH_2]$ (1.16), followed by DODAC:MO (2:1) ($[Iv C\text{-}C_G/Iv C\text{-}C_T]$=0.95 and $[Iv_aCH_2/Iv_sCH_2]$ =1.05) which means that DODAB:MO (2:1) has a more densely packed bilayer, closer to a perfect *all-trans* state.

Similar values of $[Iv_aCH_2/Iv_sCH_2]$ ratio (1.00) were found for DODAB:MO (1:2) and DODAC:MO (1:2) liposomes. Thus, when MO was in excess in the formulations (molar ratio 1:2), the presence of different counter-ions does not have an influence on the lateral packing as observed for (2:1) molar ratios. Therefore, both DODAC:MO and DODAB:MO (1:2) systems possess great content of *gauche* conformers and lower lateral packing density. Although DODAX:MO (1:2) had the same $[Iv_aCH_2/Iv_sCH_2]$ ratio, DODAC:MO (1:2) presented a slightly higher value of $[Iv C\text{-}CG/Iv C\text{-}C_T]$ than

DODAB:MO (1:2) (1.05>1.00). Hence, generally speaking and for the same molar ratio, DODAC-based liposomes have more *gauche* conformers than DODAB-based liposomes, which means that the perturbation of DODAC membranes by MO is mainly driven by a change in the *gauche/trans* ratio of the acyl chains.

Fig. 4B shows how chain decoupling (that reflects the mobility of the methyl terminal group of hydrocarbon chains) and lateral packing density of the acyl chains are related. Higher $[Iv_sCH_3/Iv_sCH_2]$ ratios indicate higher decoupling and more mobile CH_3, which increase the molar volume of the molecule.

As expected, DODAB:MO and DODAC:MO (1:2) had higher chain decoupling ratios, since that higher MO content promotes a fluidizing effect at the membrane level. We nevertheless observed that, for the same molar ratio, DODAC-based liposomes had higher $[Iv_sCH_3/Iv_sCH_2]$ values indicating a more mobile terminal methylene end group ($[Iv_sCH_3/Iv_sCH_2]$=0.62 for DODAC:MO (2.1) versus $[Iv_sCH_3/Iv_sCH_2]$=0.50 for DODAB:MO (2:1) and $[Iv_sCH_3/Iv_sCH_2]$=0.93 for DODAC:MO (1:2) versus $[Iv_sCH_3/Iv_sCH_2]$=0.88 for DODAB:MO (1:2). The higher chain decoupling obtained for DODAC based liposomes indicates that DODAC hydrocarbon chains interact less strongly than DODAB chains, especially for (1:2) molar ratio. This is in agreement with the *gauche* conformer increase observed for DODAC:MO liposomes (higher values of $[IvC\text{-}C_G/IvC\text{-}C_T]$). Langmuir π-A isotherms are also in agreement with the Raman spectroscopy data, indicating a higher packing density for DODAB:MO (2:1) than DODAC:MO (2:1) monolayers as shown by the higher compressibility modulus (Fig. 2B). This is again related to the capability of bromide counter-ions to screen the cationic head group charge better than chloride counter-ions, thus increasing the head group packing density. As a consequence, insertion of MO into DODAB bilayers is more difficult leading to demixing of the compounds into distinctive DODAB- and MO-rich domains in the corresponding mixtures. Also, in both 3D and 2D systems, the increase in MO content (DODAX:MO (1:2)), reduced the influence that the counter-ions had on the aggregate structures. Furthermore, the effect of MO content in chain decoupling is also consistent with previous results where an increase in MO content was correlated with an increase in membrane fluidity[15].

Apart from the three regions of the Raman spectra previously defined, there is another region correspondent to the ν(C=C) vibrations of unsaturated chain segments existent in MO (Fig. 1), that appears around 1660 cm^{-1} (1654 cm^{-1} for *cis* and 1669 cm^{-1} for *trans*).[43] The ν(C=C) vibration bands were clearly visible for DODAC:MO (2:1) at 1657 cm^{-1} and 1665 cm^{-1}, but were very weak or absent for the other formulations (Fig. 3 and Table 1).

This can be due to the different distribution of MO in DODAX:MO (2:1) membranes. In DODAC:MO (2:1) membranes, MO is more homogeneously distributed, thus increasing the fluidity, as observed by an increased number of *gauche* conformers and a smaller lateral packing density (Fig. 4). The smaller lateral packing density explains in turn the fact of unsaturated C=C stretching vibrations being more evident in DODAC:MO (2:1) due to higher molecular freedom. In the case of DODAB:MO (2:1) membranes, MO is more heterogeneously distributed (phase-separated), thus increasing the fluidity in the regions where it is located but imposing constraints to the neighboring DODAB lipid molecules. This can be translated into a reduced number of *gauche* conformers and in an average higher lateral packing density (Fig. 4).

Analysis of DODAX:MO mixtures in 3D assemblies by Small Angle X-ray Scattering (SAXS)

3D assemblies of DODAX:MO mixtures were also investigated by SAXS at 20 °C. SAXS curves for 40 mM DODAB (Fig. 5A) show two well-resolved Bragg peaks that can be assigned to the first and third order reflections of a lamellar structure (q3:q1=3:1).

PLEASE INSERT FIGURE 5

The first and most intense reflection at q1 of 1.73 nm^{-1} corresponds to a Bragg distance of d = 36.3 Å comprising the lipid bilayer thickness plus the enclosed water layer. The third reflection order at q3 of 5.20 nm^{-1} is much less intense and fits well with the position expected for a lamellar phase, for which the second order reflection expected at q2 = 3.46 nm^{-1} is absent.

The increase of MO content does not change the observed DODAB structure (first-order reflection at q1=1.74 nm^{-1}, and a higher-order reflection at 3q1 (q3 = 5.2 nm^{-1})). The second-order reflection expected at 2q1 (q2 at 3.5 nm^{-1}) is also absent (Figure 5A). Missing reflection orders are reported for well-defined bilayer structures and are the result of the interplay between structure and form factors.[51] If the bilayers have slightly different thicknesses, then the even-order peaks will be present. [52] This is in agreement with the fact that the DODAB assemblies are well-ordered with no bilayer thickness fluctuations.

While DODAB assemblies presented a well-ordered lamellar structure (Fig. 5A), in the same q range, SAXS scattering data of DODAC and the corresponding mixtures with MO do not show any Bragg peaks (Fig. 5B1) of a bilayer arrangement at least up to the concentrations tested in the current work (40 mM). The absence of diffraction peaks can, in this case, be associated with the formation of unilamellar vesicles (ULVs), as described previously for DODAAC (another DODAX cationic lipid where the counter-ion is the acetate) at concentrations up to 50 mM.[52] Indeed, as previously stated, the bigger hydration shell of the chloride counter-ion leads to a less effective screening of the positive charge of DODAC head groups. The charged head groups are repelled by electrostatic interactions and preferentially form ULVs that are weak scatterers compared to aligned bilayers and MLVs.[53-55]

The formation of ULVs of DODAC:MO can be confirmed by the observation of diffraction peaks at much smaller q values (Fig 5B2) with the first-order of reflection at q1 of 0.112 nm^{-1} and a higher-order reflection at q2 of 0.231 nm^{-1} that fits well with a peak position expected for the second-order reflection of a lamellar structure (q2:q1=2:1). These diffraction peaks are consistent with other SAXS diffraction studies using ULVs of 50 nm size that presented the first-order reflection at low q values (0.1 nm^{-1}).[54, 55] The Bragg peaks obtained for DODAC:MO mixtures are however

less intense and more diffuse than the ones obtained with DODAB:MO mixtures for higher q values.

From the Bragg peaks positions the values of interlayer spacing d obtained for 3D lamellar structures of DODAX:MO at different cationic lipid:neutral lipid molar ratios were calculated. In the case of DODAB:MO the introduction of MO does not significantly change the interlayer spacing of the system. Indeed, the values of the bilayer thickness plus the water layer obtained for every DODAB:MO molar ratio (d=36.0 Å) are in good agreement with previously data reported for neat DODAB without MO.[56, 57] The correlation length (ξ) of the bilayers is not affected by the inclusion of lower contents of MO (ξ = 555 Å for DODAB:MO (1:0) and DODAB:MO (2:1)), being however strongly increased for higher MO contents (ξ > 900 Å for DODAB:MO (1:1) and DODAB:MO (1:2)).

In the case of DODAC:MO much larger d-spacings and lower correlations lengths (ξ) compared to DODAB:MO are observed. In our work, the SAXS patterns of DODAC:MO (1:0). The much higher d-spacings are consistent with the previously reported study of neat DODAC, and also explained by the authors as being due to a pronounced electrostatic repulsion between the highly charged DODAC bilayers in the absence of additional electrolyte.[58] The insertion of MO into the DODAC bilayers is connected with a significant increase in the repeating distance due to an increase in the ULVs size. The addition of MO decreased also the FWHM (and consequently decreased ξ) of the diffraction peaks, which were in the case of DODAC:MO (1:0) weaker and more diffuse. This must be due to the fact that MO being a neutral lipid reduces the repulsion of DODAC head groups, which can favor the alignment of ULVs with a consequent increase of the scattering intensity.

Correlation between biophysical characteristics of the liposomes DODAX:MO, evaluated in this work and the resultant biological performance of their lipoplexes

The information gathered with all the biophysical techniques used within this work (Langmuir isotherms, BAM, IRRAS, Raman scattering and SAXS experiments) and with previously reported cryo-TEM[24] and cryo-SEM[12] validate a proposed model for DODAX:MO assemblies that depends of the counter-ion and MO content (Fig. 6).

PLEASE INSERT FIGURE 6

In the systems with smaller MO content, DODAX:MO (2:1), there is a higher influence of the counter-ion. Chloride ions are less able to effectively screen the positive charges of the cationic lipid head group in DODAC containing systems. This leads to a less ordered polar region due to stronger repulsive forces between the positively charged lipid head groups. As a result DODAC:MO (2:1) systems are less densely packed facilitating a homogeneous distribution of MO into DODAC bilayers (Fig. 6). DODAB:MO (2:1) systems are more densely packed at the head group region, and thus MO distribution within the bilayers is not as homogeneous, forming phase-separated DODAB- and MO-enriched domains (Fig. 6).

The lower screening of the positive charges of the cationic lipid head group in DODAC explains why DODAC:MO (2:1) liposomes reached total siRNA complexation at lower charge ratios (C.R. (+/-) = 2.5) when compared to DODAB:MO (2:1) liposomes (C.R. (+/-) = 5) (Fig. S1 A – supplementary information). The fact that DODAB bilayers are more densely packed and do not incorporate MO as homogeneously as DODAC bilayers also explains the higher resistance to destabilization by serum proteins achieved for DODAB:MO based lipoplexes (Fig. S1 B – supplementary information). Furthermore DODAC:MO (2:1) systems originate lipoplexes with less transfection efficiency than DODAB:MO (2:1) systems (Fig. S1 C – supplementary information). Given that both systems present the same MO content, the differences presented must be correlated with the MO distribution. MO is more homogeneously distributed in the case of DODAC bilayers, but forms phase-separated DODAB- and MO-enriched domains in DODAB based systems. These MO-enriched domains among DODAB domains might facilitate the adherence and fusion of the lipoplexes to the surfaces of the cells improving transfection.[59]

When MO was in excess in the formulations (molar ratio 1:2), the presence of different counter-ions did not have such a strong influence in terms of lateral packing as observed for (2:1) molar ratios. This indicates that saturation of bilayers with MO leads to disruption of DODAB-rich domains, making DODAB:MO and DODAC:MO bilayers more alike (Fig. 6). As previously observed by cryo-TEM[24] and cryo-SEM[12], exceeding MO seems to be excluded from the liposomal bilayer to the liposomal core where it might form MO-rich inverted non-lamellar structures (also observed by other authors in lipid mixtures containing MO[10, 60]) or MO containing vesicles (Fig. 6).

As the systems with higher MO content DODAX:MO (1:2) are similar in terms of MO distribution (Fig. 6) their performance as lipoplexes has shown to be similar as well. Hence, DODAB:MO (1:2) and DODAC:MO (1:2) based lipoplexes present comparable transfection efficiencies (Fig. S1C – supplementary information).

Conclusions

This work describes the detailed characterization of the influence of the counter-ion and MO content on DODAX:MO structural organization. The results found for DODAX:MO (2:1) systems can be summarized as follows: (i) DODAB:MO (2:1) forms bilayers more densely packed at the head group region than DODAC:MO (2:1) bilayers; (ii) MO is more homogeneously distributed in DODAC-based bilayers, but forms phase-separated DODAB- and MO-enriched domains in DODAB aggregates; (iii) Chloride and bromide counter-ions induce different repulsive interactions at the head groups' level due to differences in the surfactant hydration shell. E.g. the chloride ion has a larger hydration shell, resulting in lower screening of the positive charges of the cationic lipid head group in DODAC. This leads to a less ordered polar region due to stronger repulsive forces between the positively charged lipid head groups, facilitating a homogeneous distribution of MO into DODAC bilayers.

DODAX:MO (1:2) systems are more similar because the excess of MO reduces the effect of the counter-ion.

The differences observed between the formulations studied are correlated with key processes such as lipoplex assembly/disassembly or colloidal stability, ultimately influencing lipid-mediated transfection efficiency. Therefore, this work highlights the importance of a detailed biophysical characterization of lipoplexes' lipid components to better understand their biological outcomes and to aid scientists in the rational design of new and efficient gene therapy nanocarriers.

Acknowledgements

We acknowledge DAAD/FCT that provided the financial support required to gather the Portuguese and the German co-workers. This work was further supported by FEDER through POFC-COMPETE and by national funds from FCT, through the projects PEst-OE/BIA/UI4050/2014 (CBMA) and PEst-C/FIS/UI0607/2013 (CFUM). Marlene Lúcio acknowledges FCT for the financial support provided by the exploratory project IF/00498/2012. C.R.-A. is grateful to the European Union through the Operational Programme for Cross-border Cooperation: Spain-Portugal under Grant POCTEP 2007-2013 and to European Regional Development Fund for research funding (Innovation in Nanomedicine Project). The authors would also like to acknowledge Irina Berndt and Claudia Botelho.

References

1. T. M. Allen and P. R. Cullis, *Adv Drug Deliv Rev*, 2013, **65**, 36-48.
2. D. A. Balazs and W. T. Godbey, *Journal of Drug Delivery*, 2011, **2011**, 326497.
3. S. Zhang, Y. Xu, B. Wang, W. Qiao, D. Liu and Z. Li, *J. Control. Release*, 2004, **100**, 165-180.
4. H. Farhood, N. Serbina and L. Huang, *Biochim. Biophys. Acta*, 1995, **1235**, 289-295.
5. I. Koltover, T. Salditt, J. O. Radler and C. R. Safinya, *Science*, 1998, **281**, 78-81.
6. Y. Xu and F. C. Szoka, *Biochemistry*, 1996, **35**, 5616-5623.
7. N. J. Zuidam and Y. Barenholz, *Biochim. Biophys. Acta*, 1998, **1368**, 115-128.
8. M. J. Blandamer, B. Briggs, P. M. Cullis, B. J. Rawlings and J. B. F. N. Engberts, *PCCP*, 2003, **5**, 5309-5312.
9. F. Koster, D. Finas, C. Schulz, C. Hauser, K. Diedrich and R. Felberbaum, *Int. J. Mol. Med.*, 2004, **14**, 769-772.
10. B. Angelov, A. Angelova, M. Drechsler, V. M. Garamus, R. Mutafchieva and S. Lesieur, *Soft Matter*, 2015, **11**, 3686-3692.
11. B. Angelov, A. Angelova, S. K. Filippov, G. Karlsson, N. Terrill, S. Lesieur and P. Stepanek, *Soft Matter*, 2011, **7**, 9714-9720.
12. C. Carneiro, A. Correia, T. Collins, M. Vilanova, C. Pais, A. C. Gomes, M. E. Real Oliveira and P. Sampaio, *Eur. J. Pharm. Biopharm.*, 2015, **89**, 190-200.
13. J. P. Neves Silva, P. J. Coutinho and M. E. Real Oliveira, *J Fluoresc*, 2008, **18**, 555-562.
14. J. P. Silva, A. C. Oliveira, M. P. Casal, A. C. Gomes, P. J. Coutinho, O. P. Coutinho and M. E. Oliveira, *Biochim. Biophys. Acta*, 2011, **1808**, 2440-2449.
15. J. P. Silva, A. C. Oliveira, M. Lucio, A. C. Gomes, P. J. Coutinho and M. E. Oliveira, *Colloids Surf. B. Biointerfaces*, 2014, **121**, 371-379.
16. J. P. Silva, I. M. Oliveira, A. C. Oliveira, M. Lucio, A. C. Gomes, P. J. Coutinho and M. E. Oliveira, *Biochim. Biophys. Acta*, 2014, **1838**, 2555-2567.
17. J. P. N. Silva, A. C. N. Oliveira, L. M., A. F. C. Gomes and M. E. C. D. Real Oliveira, *J Appl Solut Chem Model*, 2014, **3**, 94-105.
18. J. P. Neves Silva, A. C. N. Oliveira, A. C. Gomes and M. E. C. D. Real Oliveira, *Development of Dioctadecyldimethylammonium Bromide/Monoolein Liposomes for Gene Delivery*, InTech, Rijeka (Croatia), 2012.
19. J. Briggs and M. Caffrey, *Biophys. J.*, 1994, **67**, 1594-1602.
20. H. Qiu and M. Caffrey, *Biomaterials*, 2000, **21**, 223-234.
21. A. Deshpande, P. Sicinski and P. W. Hinds, *Oncogene*, 2005, **24**, 2909-2915.
22. C. V. Kulkarni, W. Wachter, G. Iglesias-Salto, S. Engelskirchen and S. Ahualli, *Phys. Chem. Chem. Phys.*, 2011, **13**, 3004-3021.
23. A. Ganem-Quintanar, D. Quintanar-Guerrero and P. Buri, *Drug Dev. Ind. Pharm.*, 2000, **26**, 809-820.
24. I. M. Oliveira, J. P. Silva, E. Feitosa, E. F. Marques, E. M. Castanheira and M. E. Real Oliveira, *J. Colloid Interface Sci.*, 2012, **374**, 206-217.
25. E. Feitosa and F. R. Alves, *Chem. Phys. Lipids*, 2008, **156**, 13-16.
26. A. C. Oliveira, T. F. Martens, K. Raemdonck, R. D. Adati, E. Feitosa, C. Botelho, A. C. Gomes, K. Braeckmans and M. E. Real Oliveira, *ACS Appl Mater Interfaces*, 2014, **6**, 6977-6989.
27. P. Dynarowicz-Latka, A. Dhanabalan and O. N. Oliveira, Jr., *Adv. Colloid Interface Sci.*, 2001, **91**, 221-293.
28. M.-H. Ropers and G. Brezesinski, *Soft Matter*, 2013, **9**, 9440-9448.
29. F. Bonosi and G. Gabrielli, *Colloids and Surfaces*, 1991, **52**, 277-285.
30. A. M. Gonçalves da Silva and R. I. S. Romão, *Chem. Phys. Lipids*, 2005, **137**, 62-76.
31. K. Hąc-Wydro, P. Wydro and P. Dynarowicz-Łątka, *J. Colloid Interface Sci.*, 2005, **286**, 504-510.
32. D. M. Taylor, Y. Dong and C. C. Jones, *Thin Solid Films*, 1996, **284–285**, 130-133.
33. I. Petrov, D. Moebius and A. Angelova, *Langmuir*, 1992, **8**, 201-205.
34. E. Feitosa, F. R. Alves, E. M. S. Castanheira and M. E. C. D. Real Oliveira, *Colloid. Polym. Sci.*, 2009, **287**, 591-599.
35. C. K. Liu and G. G. Warr, *Soft Matter*, 2014, **10**, 83-87.
36. K. M. McGrath, *Langmuir*, 1995, **11**, 1835-1839.
37. V. L. Shapovalov and G. Brezesinski, *J. Phys. Chem. B*, 2006, **110**, 10032-10040.
38. M. N. Antipina, B. Dobner, O. V. Konovalov, V. L. Shapovalov and G. Brezesinski, *J. Phys. Chem. B*, 2007, **111**, 13845-13850.
39. V. Kolev, A. Ivanova, G. Madjarova, A. Aserin and N. Garti, *J. Chem. Phys.*, 2012, **136**, 074509.

40. A. P. Dabkowska, D. J. Barlow, A. V. Hughes, R. A. Campbell, P. J. Quinn and M. J. Lawrence, *J R Soc Interface*, 2012, **9**, 548-561.
41. C. B. Fox, R. A. Horton and J. M. Harris, *Anal. Chem.*, 2006, **78**, 4918-4924.
42. J. R. Beattie, S. E. Bell and B. W. Moss, *Lipids*, 2004, **39**, 407-419.
43. F. N. R. Petersen and C. H. Nielsen, *Spectroscopy*, 2009, **24**, 1-7.
44. J. M. Sanderson and A. D. Ward, *Chem. Commun.*, 2004, DOI: 10.1039/B316757G, 1120-1121.
45. K. Larsson and R. P. Rand, *Biochim. Biophys. Acta*, 1973, **326**, 245-255.
46. R. G. Snyder, S. L. Hsu and S. Krimm, *Spectrochim. Acta, Pt. A: Mol. Spectrosc.*, 1978, **34**, 395-406.
47. D. Lin-Vien, N. B. Colthup, W. G. Fateley and J. G. Grasselli, in *The Handbook of Infrared and Raman Characteristic Frequencies of Organic Molecules*, Academic Press, San Diego, 1991, DOI: http://dx.doi.org/10.1016/B978-0-08-057116-4.50008-0, pp. 9-28.
48. D. F. H. Wallach, S. P. Verma and J. Fookson, *Biochimica et Biophysica Acta (BBA) - Reviews on Biomembranes*, 1979, **559**, 153-208.
49. M. Prochazka, J. Stepanek and P. Y. Turpin, *Chem. Phys. Lipids*, 2004, **132**, 145-156.
50. R. G. Snyder, H. L. Strauss and C. A. Elliger, *The Journal of Physical Chemistry*, 1982, **86**, 5145-5150.
51. C. Suryanarayana and M. G. Norton, *X-Ray Diffraction - A pratical approach*, Springer Sciences+Business Media, 1998.
52. F. R. Alves and W. Loh, *J. Colloid Interface Sci.*, 2012, **368**, 292-300.
53. M. R. Brzustowicz and A. T. Brunger, *J. Appl. Crystallogr.*, 2005, **38**, 126-131.
54. N. Kucerka, Y. Liu, N. Chu, H. I. Petrache, S. Tristram-Nagle and J. F. Nagle, *Biophys. J.*, 2005, **88**, 2626-2637.
55. N. Kucerka, J. Pencer, J. N. Sachs, J. F. Nagle and J. Katsaras, *Langmuir*, 2007, **23**, 1292-1299.
56. E. Feitosa, R. D. Adati, P. Hansson and M. Malmsten, *PLoS One*, 2012, **7**, e44702.
57. F. G. Wu, Z. W. Yu and G. Ji, *Langmuir*, 2011, **27**, 2349-2356.
58. P. Saveyn, J. Cocquyt, M. Gradzielski and P. Van der Meeren, *Colloids Surf. Physicochem. Eng. Aspects*, 2008, **319**, 62-70.
59. B. Ma, S. Zhang, H. Jiang, B. Zhao and H. Lv, *J. Control. Release*, 2007, **123**, 184-194.
60. B. Angelov, A. Angelova, V. M. Garamus, M. Drechsler, R. Willumeit, R. Mutafchieva, P. Stepanek and S. Lesieur, *Langmuir*, 2012, **28**, 16647-16655.
61. C. J. Orendorff, M. W. Ducey and J. E. Pemberton, *The Journal of Physical Chemistry A*, 2002, **106**, 6991-6998.

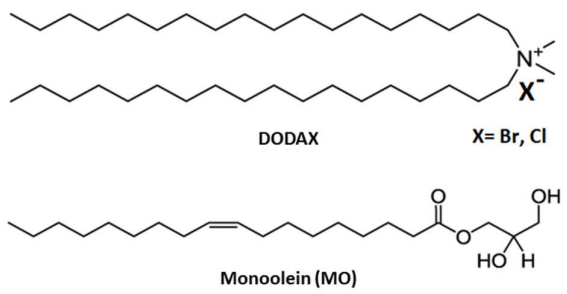

Fig. 1 Chemical structures of DODAB/DODAC and monoolein (MO) lipids.

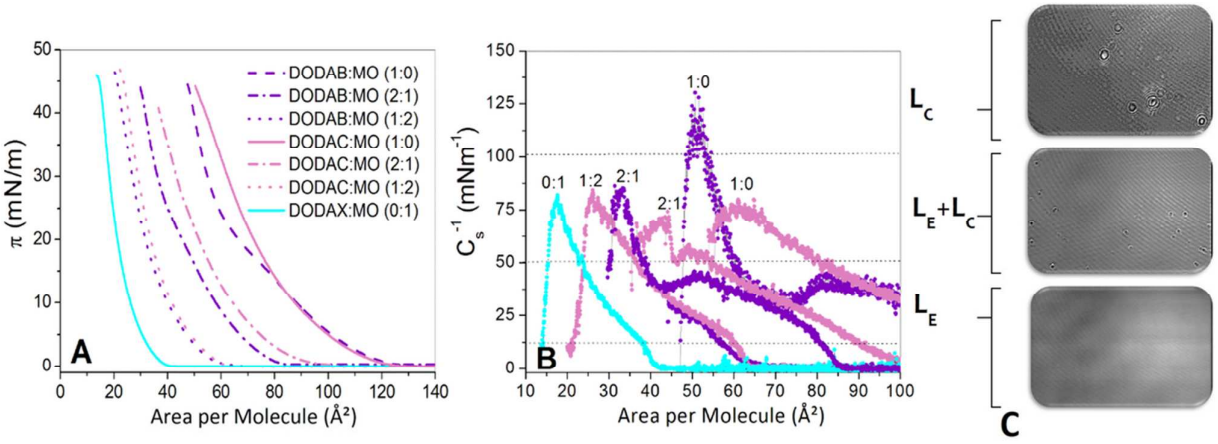

Fig. 2 (**A**) - Surface pressure-molecular area (π-A) isotherms (20 °C, aqueous subphase) of DODAX (DODAB or DODAC) and MO monolayers as well as of mixed monolayers at different DODAX:MO molar ratios (0:1, 1:0, 2:1, and 1:2). (**B**) - Compression modulus (C_s^{-1}) calculated from the isotherms presented in (A). Pink stand for DODAC based monolayers, purple colors stand for DODAB based monolayers, and blue color stands for the MO monolayer. The regions of the liquid-condensed phase (L_C), of the coexistence between liquid-condensed and liquid-expanded phases (L_E+L_C), and of the liquid-expanded phase (L_E) are marked. (**C**) - BAM images of DODAB monolayer on an aqueous subphase in the different regions L_E, L_E+L_C and L_C.

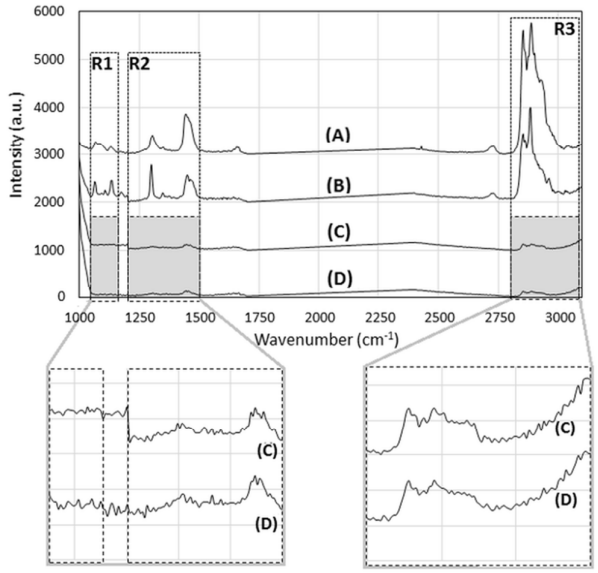

Fig. 3. Raman spectra of DODAC:MO (2:1) (**A**), DODAB:MO (2:1) (**B**), DODAC:MO (1:2) (**C**) and DODAB:MO (1:2) (**D**) liposomes. Insets show the spectra of DODAC:MO (1:2) (C) and DODAC:MO (1:2) (D) with regions R1, R2 and R3 in more detail.

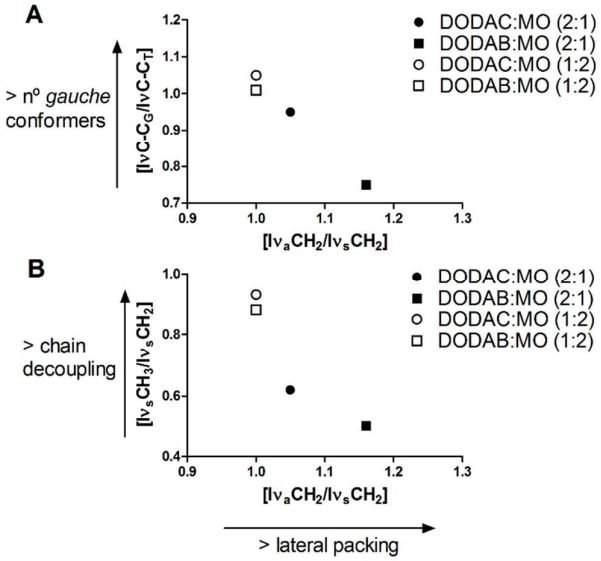

Fig. 4 Intensity ratio [I $\nu C\text{-}C_G$/I $\nu C\text{-}C_T$] as function of [I $\nu_a CH_2$/I $\nu_s CH_2$] (**A**) and [I $\nu_s CH_3$/I $\nu_s CH_2$] as function of [I $\nu_a CH_2$/I $\nu_s CH_2$] (**B**).

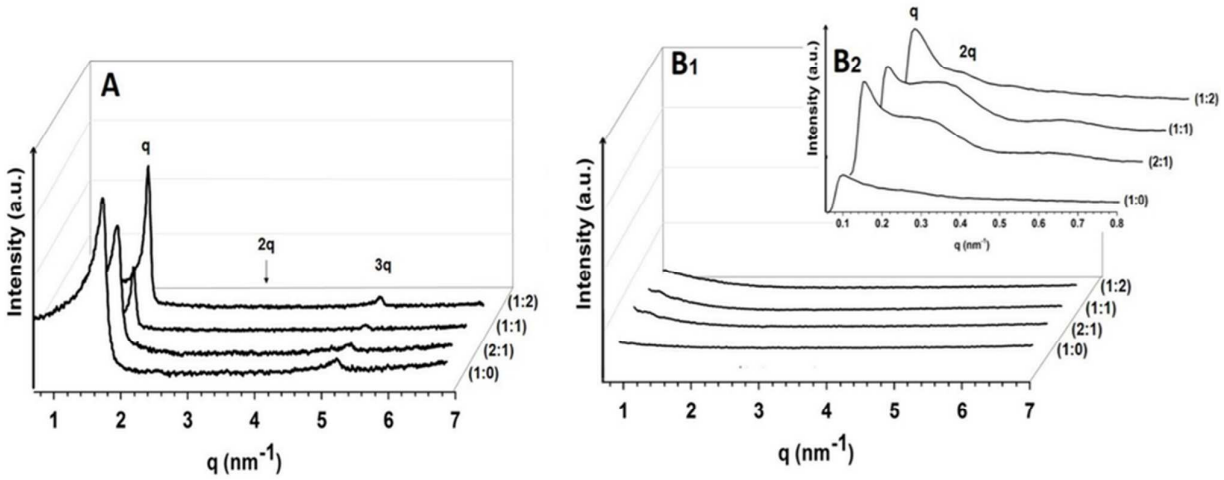

Fig. 5 A - SAXS curves for DODAB:MO (40 mM) in water at 20 °C, obtained at (1:0); (2:1); (1:1) and (1:2) ratios. **B** - SAXS curves for DODAC:MO (40 mM) in water at 20 °C, obtained at (1:0); (2:1); (1:1) and (1:2) ratios at higher q values (B_1) and at lower q values (B_2). q, 2q and 3q indicate the first-, second- and third-order of reflection.

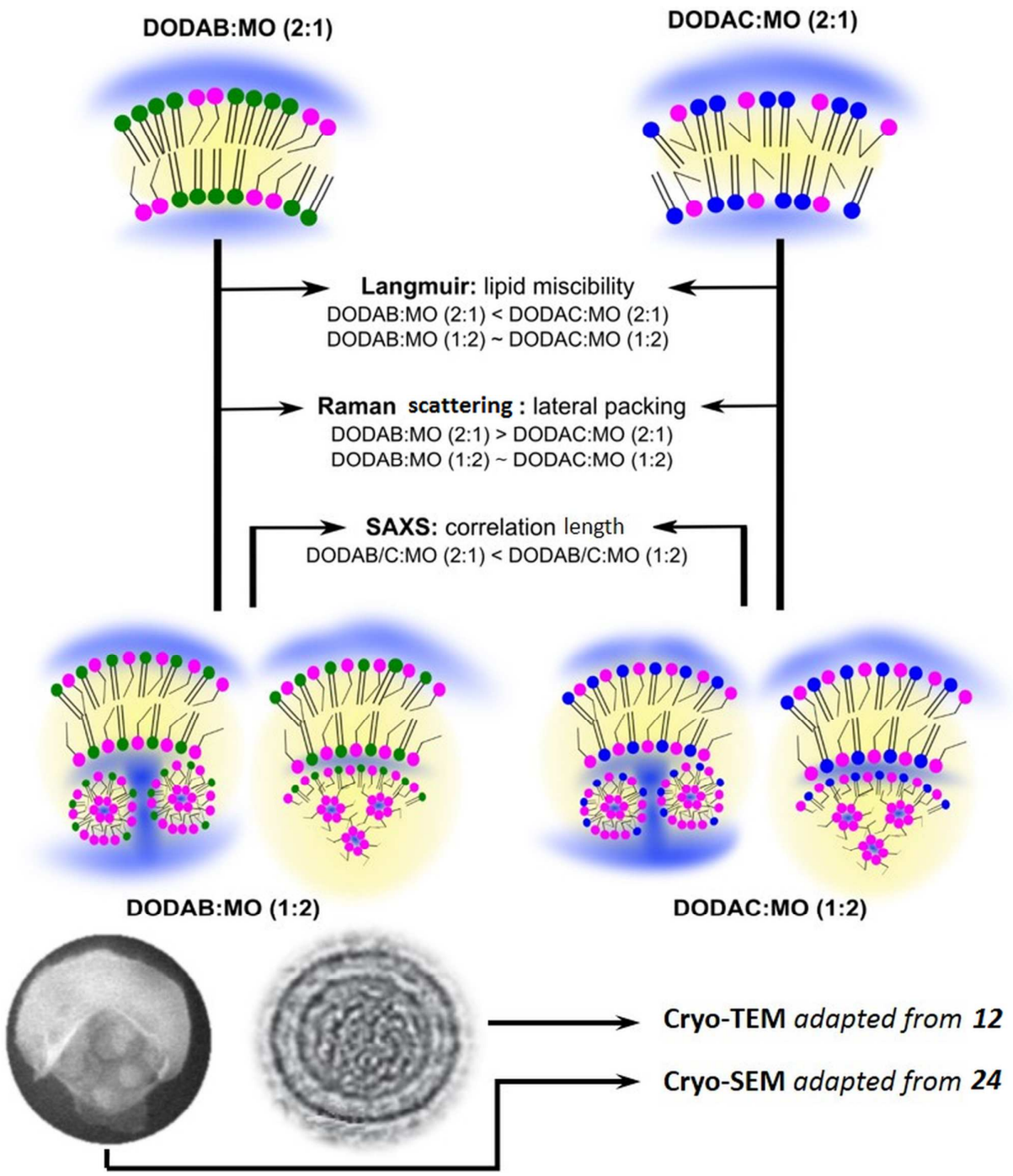

Fig. 6 Schematic representation of the main results obtained for DODAB:MO (2:1), DODAC:MO (2:1), DODAB:MO (1:2) and DODAC:MO (1:2) liposomes by Langmuir isotherms, Raman scattering and SAXS experiments. Previously reported cryo-TEM[24] and cryo-SEM[12] micrographs of DODAB:MO with high MO ratios validate the proposed model.

Table 1. Experimental Raman band frequencies (cm^{-1}) and respective assignments.[42, 61]

	DODAC:MO (2:1)	DODAB:MO (2:1)	DODAC:MO (1:2)	DODAB:MO (1:2)	Assignment*
R1 C-C stretching region	1068	1066	1068	1064	$\nu(C\text{-}C)_T$
	1083	1084	1085	1088	$\nu(C\text{-}C)_G$
	1107/1135	1109/1135	1107/1134	1107/1134	$\nu(C\text{-}C)_{ip}$
R2	1305	1301	-	-	$\delta(CH_2)_{tw}$
C-H deformation region	1440/1448/ 1462	1450/1464/ 1474	1438/1446/ 1464/1484	1438/1445/ 1458/1476	$\delta(CH_2)_{sc}$
	1657/1665	1646/1667	-	1644/1667	$\nu(C{=}C)$
R3 C-H stretching region	2855	2855	2855	2855	$\nu_s(CH_2)$
	2888	2885	2889	2884	$\nu_a(CH_2)$
	2935	2935	2935	-	$\nu_s(CH_3)$
	2965	2963	-	2962	$\nu_a(CH_3)$

*ν – stretch; δ – bend and or scissor/deformations. T – *trans*, G – *gauche*, ip – in-phase, tw – twist, sc – scissor, s – symmetric, a – antisymmetric.

Supplementary Information

Role of counter-ion and helper lipid content in the performance of nanocarrier systems: a biophysical study in 2D and 3D lipid assemblies

Ana C. N. Oliveira[a,b], Sara S. Nogueira[b,c], Odete Gonçalves[a,b], M. F. Cerqueira[b], P. Alpuim[b,d], Júlia Tovar[b], Carlos Rodriguez- Abreu[d], Gerald Brezesinski[c], Andreia C. Gomes[a], Marlene Lúcio[b], M.E.C.D. Real Oliveira[b]*

[a]CBMA (Centre of Molecular and Environmental Biology), Department of Biology, University of Minho, Campus of Gualtar, 4710-057 Braga, Portugal

[b]CFUM (Centre of Physics), Department of Physics, University of Minho, Campus of Gualtar, 4710-057 Braga, Portugal

[c]Max Planck Institute of Colloids and Interfaces, Science Park Potsdam-Golm, 14476 Potsdam, Germany

[d]INL (International Iberian Nanotechnology Laboratory), Av. Mestre José Veiga, 4715-330 Braga, Portugal

Corresponding Author

*Marlene Lúcio

E-mail: mlucio@fisica.uminho.pt, Department of Physics, University of Minho, Campus of Gualtar, 4710-057 Braga, Portugal. Tel: 253604060, Fax: 253604061

siRNA complexation, serum stability and silencing efficiency of DODAX:MO systems.

Depending on the counter-ion DODAX:MO (2:1) systems have shown differences in the % of siRNA complexation; in the serum stability of lipoplexes and differences in transfection efficiency (Fig. S1).

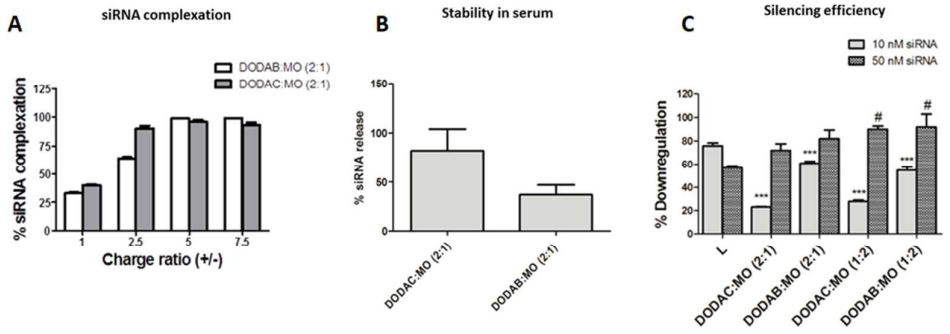

Fig. S1. Influence of counter-ion and MO content on siRNA complexation of DODAX:MO (2:1) liposomes (A), on the capacity of DODAX:MO (2:1) based lipoplexes to retain siRNA content in human serum (B) and on the transfection efficiency of DODAX:MO based lipoplexes. The percentage of RNA complexation after addition of DODAB:MO and DODAC:MO (2:1) liposomes to a RNA solution, was evaluated with the RNA intercalating probe Ribogreen. The stability in serum and silencing efficiency were adapted from[26].

To illustrate the impact of the counter-ion on the lipoplex formation, siRNA complexation was studied at different charge ratios C.R. (+/-) by the RiboGreen fluorimetric assay, according to the manufacturer specifications. Briefly, lipoplexes were incubated with RiboGreen solution in the dark (5 min) and then the fluorescence was measured in a Fluoroskan ACEN FL Microplate Fluorometer and Luminometer (Thermo Scientific, Waltham, MA), using the excitation/emission filter pair of 485/538 nm. A calibration curve was made in order to assure the linearity between the RiboGreen fluorescence and RNA concentration. The percentage of free RNA was attained from a control, of the same quantity of RNA used in the preparation of the lipoplexes. DODAC:MO (2:1) liposomes reached total siRNA complexation at lower C.R.

(+/-) = 2.5 comparing to DODAB:MO (2:1) liposomes that needed higher C.R. (+/-) = 5 to reach total siRNA complexation (Fig. S1 A). The colloidal stability of DODAX:MO (2:1) in human serum has been previously studied and has also shown to be dependent on the counter-ion (Fig. S1 B). [26] DODAB:MO (2:1) based lipoplexes are more stable in serum than DODAC:MO (2:1) based lipoplexes. Finally both the MO content and the counter-ion have influence in silencing efficiency, as stated in our previous study. [26] Lipoplexes based on DODAB systems with low MO content (DODAB:MO (2:1)) are more efficient in gene silencing than DODAC:MO (2:1) based lipoplexes (Fig. S1 C). At higher MO contents (1:2), the counter-ion influence is very much reduced and gene silencing is similar for lipoplexes based on DODAB:MO or DODAC:MO.

Infrared reflection-absorption spectroscopy (IRRAS) to evaluate phase transition of DODAB, DODAC and MO monolayers

IRRAS is a powerful tool to obtain a widespread spectrum of information of lipid monolayers at the air–water interface and by the position of the CH_2 symmetric, $\nu_s(CH_2)$, and asymmetric, $\nu_{as}(CH_2)$, stretching bands the phase state of lipids can be determined. LE phases are characterized by asymmetric, $\nu_{as}(CH_2)$, stretching bands around 2925 cm^{-1}, respectively, while in the LC phase, these bands are shifted to lower wavenumbers (2920 cm^{-1}). Accordingly, Figure S2 shows the position of $\nu_{as}(CH_2)$ of DODAB, DODAC and MO at different pressures in a aqueous subphase and 20 ºC. The phase transition from LE to LC in DODAB monolayers is connected with a jump in the wavenumbers of the CH_2¬ stretching vibrations to lower values indicating a clear phase transition as observed in the π-*A* isotherms. In the case of DODAC the transition to the LC phase cannot be observed and the wavenumbers decrease continuously with increasing pressure. At the highest lateral pressure measured, the wavenumbers of DODAC are at least 1 cm^{-1} larger than those of DODAB indicating a less dense packing. MO, as expected, presented a LE phase with no transition.

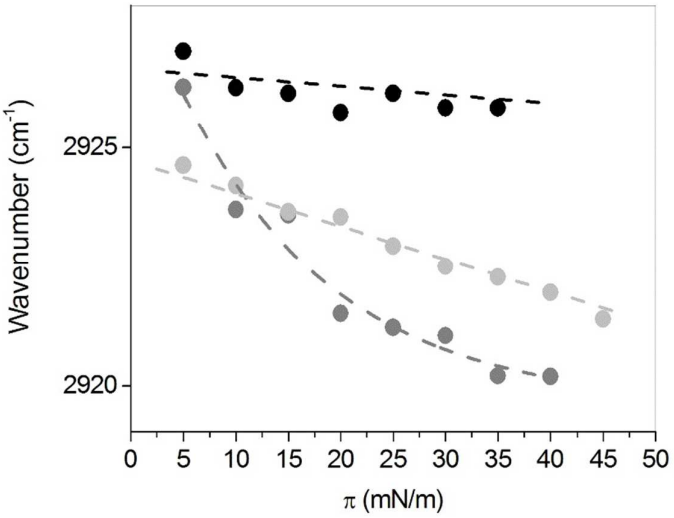

Fig. S2- Position of the asymmetric CH_2-stretching vibration of DODAB (dark grey dots), DODAC (light grey dots) and MO (black dots) on aqueous subphase at 20 °C in dependence of the surface pressure.

Langmuir isotherms of DODAB and DODAC on 10 mM NaBr or NaCl subphases

To illustrate the counter ion effect, DODAB and DODAC have been measured on 10 mM NaBr or NaCl solutions, respectively. In the case of DODAB, the phase transition region (coexistence of LE and LC) is seen as a perfect horizontal plateau at ~2 mN/m, whereas DODAC on the 10 mM NaCl solution does not exhibit any plateau but the area decreases continuously with increasing pressure. Above 20 mN/m, the molecular area of DODAC is smaller than that of DODAB indicating a less dense packing in DODAC.

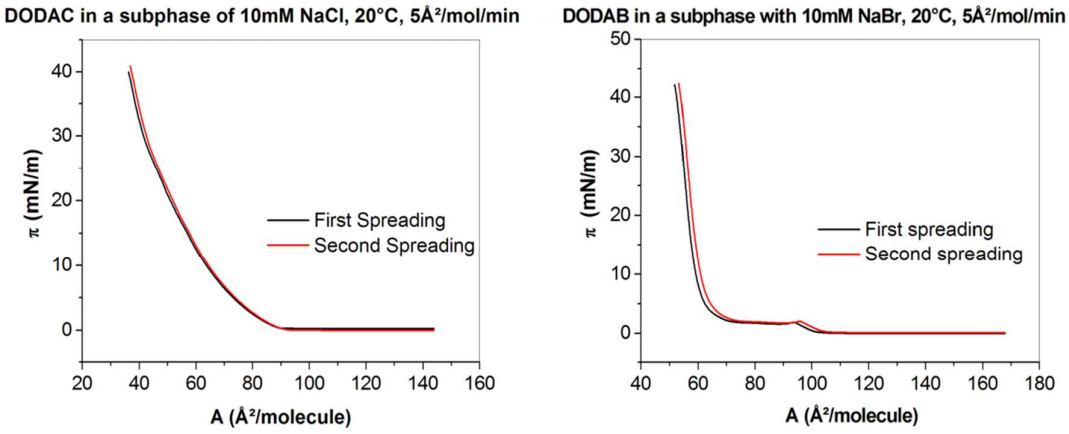

Fig. S3- Surface pressure-molecular area (π-A) isotherms (20 °C, aqueous subphase containing 10 mM of NaCl or NaBr) of DODAC (left) and DODAB (right) monolayers.

Brewster Angle Microscopy (BAM) of DODAB:MO and DODAC:MO (2:1)

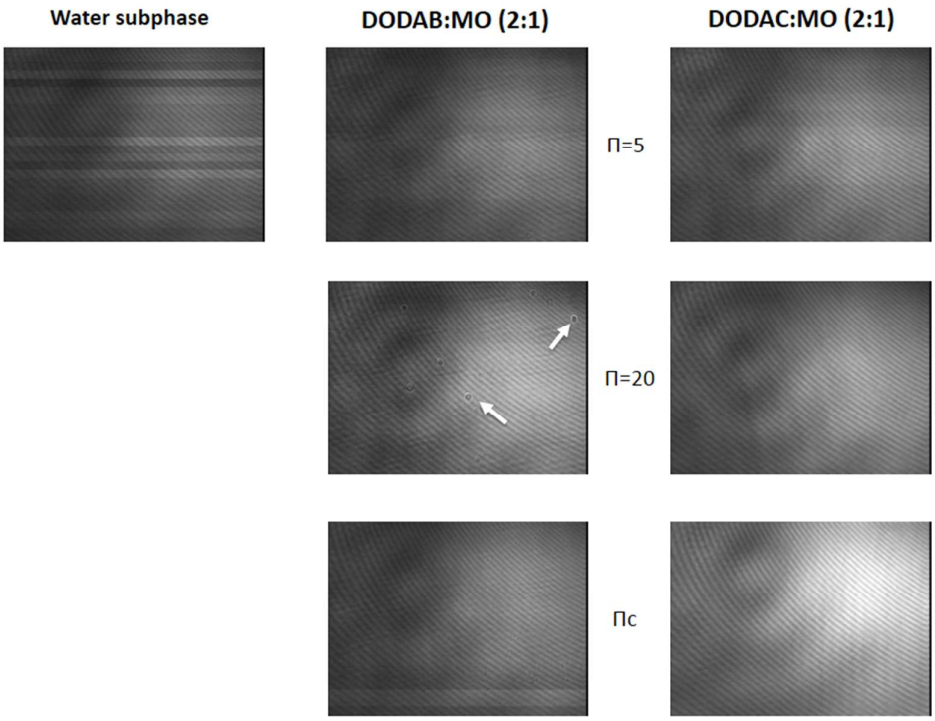

Fig. S4- BAM images of DODAB:MO and DODAC:MO (2:1) monolayer on an aqueous subphase at different pressures. Arrows indicate the presence of presence of small domains showing 'bubble-like' features in DODAB mixed monolayers that do not appear in DODAC mixed monolayers.